TRI-LINEAR MODEL FOR THE OUT-OF-PLANE SEISMIC ASSESSMENT OF VERTICALLY-SPANNING UNREINFORCED MASONRY WALLS

Michele Godio[1] and Katrin Beyer[2]

[1]Postdoctoral Researcher, Earthquake Engineering and Structural Dynamics Laboratory (EESD), School of Architecture, Civil and Environmental Engineering (ENAC), École Polytechnique Fédérale de Lausanne (EPFL), EPFL ENAC IIC EESD, GC B2 495, Station 18, CH-1015 Lausanne, Switzerland. Email: michele.godio@epfl.ch

[2]Associate Professor, Earthquake Engineering and Structural Dynamics Laboratory (EESD), School of Architecture, Civil and Environmental Engineering (ENAC), École Polytechnique Fédérale de Lausanne (EPFL), EPFL ENAC IIC EESD, GC B2 495, Station 18, CH-1015 Lausanne, Switzerland. Email: katrin.beyer@epfl.ch

ABSTRACT

Out-of-plane failure of masonry walls is often responsible for the partial collapse of unreinforced masonry structures. Modeling the out-of-plane response of these walls is therefore key in the assessment of existing buildings. The paper presents a new tri-linear model describing the force-displacement response of vertically-spanning unreinforced masonry walls subjected to out-of-plane loading. Different factors that affect the response of the walls are captured by the model: the support conditions, the level of applied axial load, the slenderness ratio and the deformability of the wall. The model is validated against experimental results from shake table tests. The force and displacement parameters of the model are described by analytical expressions that are derived from a mechanical model previously developed for unreinforced masonry. They offer an alternative to existing tri-linear models where corner displacements are mainly defined by empirical relationships.

Keywords: URM wall, out-of-plane loading, tri-linear model, one-way bending, rocking, NTHA

INTRODUCTION

Vertically-spanning, or one-way bending, unreinforced masonry (URM) walls are among the most vulnerable walls against out-of-plane failure mechanisms, as observed in post-earthquake surveys carried out on commercial and residential buildings (Giaretton et al. 2016a). This type of failure mechanism is usually observed in long walls, or in walls without side supports. Moreover, cantilever, or overturning, types of failure, which are also part of this class of out-of-plane failure mechanisms, mainly due to a lack of top horizontal restraint, are by far the most commonly observed failure mechanisms in URM buildings (D'Ayala and Speranza 2003).

The seismic behavior of vertically-spanning URM walls undergoing large out-of-plane deflections and rocking can be described by simplified force-displacement models such as the bi-linear model and the tri-linear model (Doherty 2000; Doherty et al. 2002; Griffith et al. 2003; Sorrentino et al. 2016), see Fig. 1. Bi-linear models are derived from non-linear rigid-body kinematic analysis of the wall, i.e., by modeling the wall as one or several rigid macroblocks, which are separated by fully cracked cross-sections and undergo large relative displacements and rotations. The non-linear kinematic analysis yields the two parameters of the model, which are the force F_0 and the displacement Δ_0. Tri-linear models are derived when the deformability of the masonry is taken into account. These models are composed of a first linear increasing branch, a horizontal plateau and a third branch that follows the descending branch obtained by non-linear kinematic analysis. The tri-linear model is defined by the force parameter F_1, that is the force at the plateau level, the displacement parameters Δ_1, Δ_2 and the ultimate displacement Δ_U. The parameters of the tri-linear model are usually related to those of the bi-linear model through the ratios F_1/F_0 and Δ_1/Δ_0, Δ_2/Δ_0, Δ_U/Δ_0.

Due to their relative simplicity and the small computational cost, these simplified force-displacement models have gained increasing attention and are nowadays recommended by building codes for the out-of-plane assessment of URM walls when subjected to seismic loading (Sorrentino

et al. 2016). Assessment of the out-of-plane capacity of URM walls according to today's codes is based on the use of bi-linear models (NTC 2008; NZSEE 2014). Estimates of Δ_2/Δ_0 are required for predicting the displacement demand on the walls, which is obtained from an equivalent linear elastic single-degree-of-freedom system with a stiffness equal to the secant stiffness K_2, Fig. 1 (Doherty et al. 2002; Griffith et al. 2003; Sorrentino et al. 2016; Derakhshan et al. 2017). If non-linear time-history analyses are carried out, the tri-linear model shows itself particularly adapted (Sorrentino et al. 2016): unlike the bi-linear model, in addition to the displacement capacity of the wall Δ_{max}, it is able to capture the initial stiffness K_{in}, through K_1, and the force capacity F_{max}, through F_1 (Fig. 1).

Tests showed that four factors affect the response of out-of-plane vertically-spanning URM walls (Lam et al. 1995; Doherty 2000; Griffith et al. 2004; Dazio 2009; Derakhshan et al. 2014; Ferreira et al. 2015; Graziotti et al. 2016; Giaretton et al. 2016b): a) the support conditions of the wall (kinematic boundary conditions), b) the level and the eccentricity of the applied axial load (static boundary conditions), c) the height-to-thickness ratio of the wall (wall slenderness) and d) the deformability of the wall, which is given by the elastic deformation of the masonry together with its limited tensile and compressive strength. These findings were corroborated by a number of numerical and analytical studies carried out on URM walls (Lu et al. 2004; Brencich et al. 2008; Morandi et al. 2008; Cavaleri et al. 2009; Tondelli et al. 2016; Godio and Beyer 2017).

Non-linear rigid-body analysis yields insights into the influence of the static and kinematic boundary conditions and wall slenderness on the wall force capacity F_{max}. It also allows investigating the influence of these factors on the wall displacement capacity Δ_{max} (Griffith et al. 2003). However, it disregards the effect of the elastic deformation of the wall, which, together with the local rounding of the brick corners due to local crushing and the reduction of the mortar layer over the wall thickness (mortar pointing), reduces the peak force F_1 of the URM wall (Priestley 1985; Doherty 2000; Griffith et al. 2003; Derakhshan et al. 2013a; Derakhshan et al. 2014).

Tri-linear models were formulated with the aim of bounding the force capacity of the walls. The use of tri-linear models for modeling the response of vertically-spaning URM walls was introduced

in the early 2000s (Doherty 2000) and their potential has been well demonstrated by the growing number of works devoted to the topic (Table 1). Nonetheless, the tri-linear models proposed in the previous works were based on the use of the non-linear rigid-body analysis in conjunction with experimentally determined empirical parameters or ratios.

The objective of this paper is to offer fully analytical and mechanically-based formulations for the force and displacement parameters of the tri-linear model, to be used for modeling the out-of-plane response of a wide range of wall configurations without the use of empirical parameters. The new tri-linear model proposed in this paper is an engineering approximation of a recent mechanical model (Godio and Beyer 2017), which yielded the analytical expression of the experimental pushover curve for vertically-spanning URM walls subjected to out-of-plane static loading. As the model on which it is based, the herein presented tri-linear model regards masonry as a deformable homogeneous material with zero tensile strength and linear elastic constitutive law in compression. Its formulation includes the effect of geometric non-linearities. Following these assumptions, vertical strips of URM walls are modeled as deformable second-order Euler-Bernoulli beam elements where, as the wall deflects, cross-sections remain plane in the compressed regions of the wall and diffuse cracking occurs and spreads within the regions of maximum bending moment (Fig. 2). When describing the pushover curve of URM walls, idealizations of this kind yield important differences with respect to the rigid-body idealizations that are usually carried out. In particular, the following features of the experimental force-displacement curve are captured: (i) the initial slope of the curve, related to the initial elastic stiffness of the wall; (ii) the progressive reduction of the slope up to the peak force, due to the decrease of the effective thickness of the wall after cracking and the geometric non-linearity; (iii) the peak force which, because of the combined effect of wall deformability and geometric non-linearity, is always smaller than the 'rigid threshold' F_0 (Godio and Beyer 2017).

The analytical formulations presented in this paper describe the effect of the four factors experimentally observed to affect the response of out-of-plane loaded walls. The tri-linear model is formulated for three different boundary conditions (Fig. 2). The boundary conditions that are applied by the model are those offered by the beam theory (Chapman and Slatford 1957; Godio

and Beyer 2017), used here to reproduce typical support conditions observed in existing buildings (Doherty et al. 2002; Dazio 2009): URM walls spanning vertically between two supports are modeled as clamped-clamped or pinned-clamped beams, depending whether the connection with the rest of the building is provided at the top of the wall by a slab (Fig. 2(a)) or by a timber beam (Fig. 2(b)); walls laid on one single support are modeled as cantilever beams (Fig. 2(c)). For all the considered boundary conditions, the effect of the self-weight and of the level of applied axial load (overburden) is taken into account by the formulation. For walls spanning between two supports, when the axial load is small compared to the wall self-weight, the middle crack tends to form in the upper half of the wall; if the self-weight is negligible compared to the applied axial load the crack forms at mid-height (Sorrentino et al. 2008). The new model includes a formula for predicting the position of the middle crack and its effect on the force and displacement capacity of the wall is captured by the analytical expressions of the force and displacement parameters of the tri-linear model. The model captures the effect of the applied axial load also at higher levels, that is, when it is close to Euler's critical load of the wall. It is known that increasing the slenderness and decreasing the masonry elastic modulus diminishes Euler's critical load and, as a result, walls become more vulnerable to lateral loading. As such, the analytical formulations of the new tri-linear model include the effect of the elastic deformability of the walls not only on their initial stiffness K_{in}, but also on their force capacity F_{max} and displacement capacity Δ_{max}. This aspect was excluded in early tri-linear models.

The paper is organized as follows. The analytical formulations for the force and displacement parameters of the tri-linear model are first detailed. The tri-linear model is next validated against displacement time-histories obtained from laboratory shake table tests and its performance is compared to that of existing tri-linear models. The force and displacement parameters of the tri-linear model are next studied and compared with the empirical values previously suggested in the literature.

MODEL FORMULATION

The wall under consideration has a height H_{w}, a length L_{w} and a thickness t_{w}. It is subjected

to a vertical load O (overburden) and to its self-weight W (Fig. 2). The elastic modulus of the masonry is E_m and its mass density ρ. The moment of inertia of a generic uncracked cross-section of the wall is $I_\mathrm{w} = 1/12 L_\mathrm{w} t_\mathrm{w}^3$. The scheme followed for the derivation of the tri-linear model can be summarized as follows (Fig. 3):

- first, the parameters of the bi-linear model F_0 and Δ_0 are derived from the non-linear kinematic analysis of the walls undergoing rigid-body mechanisms;
- next, the plateau force F_1 is equated to the force capacity F_max of the pushover curve and expressed through the ratio F_1/F_0;
- similarly, the stiffness K_1 of the initial branch of the tri-linear model is defined as a percentage of the initial stiffness of the pushover curve K_in;
- the descending branch of the bi-linear curve is shifted in order to consider the effective thickness of the wall and the ultimate displacement Δ_U is expressed as a percentage of Δ_0;
- finally, the displacement parameters of the tri-linear model Δ_1 and Δ_2 are derived from the expressions of F_1, K_1 and Δ_U and expressed through the ratios Δ_1/Δ_0 and Δ_2/Δ_0.

The steps listed above are detailed below in this section. In the resulting expressions, Δ refers to the displacement of the control point of the wall, which corresponds to the wall mid-height for the clamped-clamped and the pinned-clamped wall and to the wall top for the cantilever or parapet wall (Fig. 2). The expressions are parametrized through the factors ϵ, β and κ, which take the following values: $0, 0.5, 0.5$ for the clamped-clamped wall; $0.5, 0.5, 0.7$ for the pinned-clamped wall; $1, 1, 2$ for the cantilever wall.

Bi-linear model parameters F_0 ***and*** Δ_0

The parameters of the bi-linear model are derived for a wall under a uniformly distributed load. The demonstration is given in Section S1 of Supplemental Data. Assuming the rigid-body mechanisms of Fig. 2, the parameters F_0 and Δ_0 result in the expressions:

$$F_0 = \frac{1}{2\beta^2} \frac{\xi W + (1-(1-\xi)\epsilon) O}{\xi(1-\xi)} \frac{t_\mathrm{w}}{H_\mathrm{w}}, \tag{1}$$

and:

$$\Delta_0 = \frac{1}{2}\frac{\xi W + (1-(1-\xi)\epsilon)O}{(1-\xi)(\xi W + O)} t_{\mathrm{w}}, \tag{2}$$

where ξ describes the position of the middle crack along the height of the wall. For clamped-clamped and pinned-clamped walls, the middle crack does not necessarily form at the wall mid-height but at $(1-\xi)H_{\mathrm{w}}$ from the base support, with ξ given by:

$$\xi = \frac{\sqrt{(1-\epsilon)(W+O)O} - (1-\epsilon)O}{W + \epsilon O}. \tag{3}$$

When the wall self-weight is little as compared to the overburden, that is $W/O \rightarrow 0$, the middle crack tends to form at $0.5H_{\mathrm{w}}$ from the base of the clamped-clamped wall and at $0.586H_{\mathrm{w}}$ from the base of the pinned-clamped walls. In these cases, the parameters of the bi-linear model are respectively $F_0 = 8Ot_{\mathrm{w}}/H_{\mathrm{w}}, \Delta_0 = t_{\mathrm{w}}$ and $F_0 = \left(3+2\sqrt{2}\right)Ot_{\mathrm{w}}/H_{\mathrm{w}}, \Delta_0 = \left(1+\sqrt{2}\right)t_{\mathrm{w}}/4$. For cantilever walls, the crack always forms at the base of the wall. In this case, the expressions for F_0 and Δ_0 are retrieved by treating ξ as an auxiliary factor set equal to $1/2$.

Force parameter F_1

The force capacity F_{max} of a vertically-spanning wall subjected to an uniformly distributed load can be approximated by Eq. (4) (Godio and Beyer 2017). Starting from this expression, the tri-linear model is built by equating the plateau force F_1 to F_{max} as proposed by Griffith et al. (2003), thus obtaining:

$$\frac{F_1}{F_0} = 1 - \left(\frac{P}{P_{\mathrm{E}}}\right)^{0.4}. \tag{4}$$

In this equation F_0 is given by Eq. (1), P is denoted as the effective axial load and is defined as (Godio and Beyer 2017):

$$P = \beta W + O, \tag{5}$$

174 and P_{E} is the Euler's critical load of the wall:

$$P_{\mathrm{E}} = \frac{\pi^2 E_{\mathrm{m}} I_{\mathrm{w}}}{(\kappa H_{\mathrm{w}})^2}. \tag{6}$$

175 The expression F_1/F_0 contained in Eq. (4) was originally derived for walls in which the middle
176 crack forms at mid-height (Godio and Beyer 2017). Finite element simulations reported in Section
177 S2 of Supplemental Data show that the same expression yields a very good approximation for walls
178 in which the middle crack does not form at mid-height but in their upper half as a result of the
179 influence of the wall self-weight on the wall response.

180 ***Stiffness*** K_1

181 Denoted with K_{in} is the initial stiffness of the wall, which was derived by Godio and Beyer
182 (2017) for a geometrically non-linear Euler-Bernoulli beam with uncracked cross-sections. Here it
183 is written as the product between the stiffness K_{lin} of a geometrically linear beam and the function
184 Ψ_K embodying the $P-\Delta$ effect:

$$K_{\mathrm{in}} = K_{\mathrm{lin}} \Psi_K. \tag{7}$$

185 The stiffness K_{lin} is classically expressed as:

$$K_{\mathrm{lin}} = \frac{\zeta E_{\mathrm{m}} I_{\mathrm{w}}}{H_{\mathrm{w}}^3}, \tag{8}$$

186 with $\zeta = 384, 192, 8$ respectively for the clamped-clamped, pinned-clamped and cantilever walls,
187 whereas the function Ψ_K can be reasonably approximated by the short form (Section S3 of Supple-
188 mental Data):

$$\Psi_K = 1 - \frac{P}{P_{\mathrm{E}}}, \tag{9}$$

where P and P_{E} are expressed for each boundary condition by Eq. (6) and (5). Ψ_K decreases linearly with increasing P/P_{E} and so does the stiffness of the wall K_{in}, which tends to K_{lin} for $P \to 0$ and to 0 for $P \to P_{\mathrm{E}}$. Once the initial elastic stiffness of the pushover curve is defined, the stiffness K_1 of the first branch of the tri-linear model is set equal to:

$$K_1 = 0.7K_{\mathrm{in}}. \tag{10}$$

The factor 0.7 defines the ratio of the effective stiffness up to Δ_1 to the initial stiffness at zero displacement.

Ultimate displacement Δ_U

The ultimate displacement of the pushover curve of URM walls is often observed to be smaller than Δ_0 obtained by the rigid-body analysis (Griffith et al. 2003; Lagomarsino 2015). Reduction of the ultimate displacement in URM walls can be due to different material and geometrical factors, namely: the rounding of the unit corners due to local deformation (Lagomarsino 2015), the unit or mortar crushing (Derakhshan et al. 2013b), a reduced effective depth of the mortar layer due to mortar pointing or due to the dropping out of mortar during the rocking of the wall (Doherty 2000; Derakhshan et al. 2013b). In order to take into account this reduction, an effective thickness of the wall $t_{\mathrm{w,eff}}$ is introduced. Expressed as $t_{\mathrm{w,eff}} = \tau t_{\mathrm{w}}$ and substituted into Eq. (1) and (2), it leads to a shift of the descending branch of the bi-linear model (Fig. 3), which results in:

$$\frac{\Delta_{\mathrm{U}}}{\Delta_0} = \tau. \tag{11}$$

Moreover, replacing t_{w} with $t_{\mathrm{w,eff}}$ in the formulation of the tri-linear model affects through I_{w} the formula for P_{E} (Eq. (6)) and K_{lin} (Eq. (8)).

Displacement parameters Δ_1 ***and*** Δ_2

The displacement parameter Δ_1 can be obtained from the expression of the plateau force F_1 (Eq. (4)) and the stiffness K_1 (Eq. (10)) as Δ_1 is defined as: $\Delta_1 = F_1/K_1$. Normalized with respect

211 to Δ_0, it writes:

$$\frac{\Delta_1}{\Delta_0} = \left[1 - \left(\frac{P}{P_{\mathrm{E}}}\right)^{0.4}\right] \frac{F_0}{\Delta_0} \frac{1}{0.7K_{\mathrm{in}}}. \tag{12}$$

212 The displacement parameter Δ_2 can be derived as $\Delta_2 = (\tau - F_1/F_0)\Delta_0$. Introducing Eq. (4), the
213 ratio of Δ_2/Δ_0 becomes:

$$\frac{\Delta_2}{\Delta_0} = \tau - 1 + \left(\frac{P}{P_{\mathrm{E}}}\right)^{0.4}. \tag{13}$$

214 ## MODEL INTEGRATION

215 The tri-linear model is integrated numerically as single-degree-of-freedom system with non-
216 linear elastic behavior following the tri-linear $F(\Delta)$ relationship. For this purpose, two assumptions
217 are required, see Fig. 2. The first assumption consists in assuming that the bottom and top
218 supports of the URM wall experience the same out-of-plane ground acceleration $a_g(t)$. The second
219 assumption consists in assuming a piece-wise linear inertia force distribution along the wall height.
220 The fist assumption represents a simplification in the case of real buildings, as the upper storeys
221 of the building may experience motions which are filtered by the building structure, i.e. the
222 walls and the diaphragms, and can therefore be different from storey to storey. Even though
223 examples of tri-linear models considering the diaphragm deformation can be found in the literature
224 (Derakhshan et al. 2015; Landi et al. 2015), a systematic study quantifying the vulnerability of
225 out-of-plane walls subjected to the relative support motion is still missing. The second assumption
226 has been corroborated by experimental observations from laboratory shake table tests (Doherty
227 2000; Graziotti et al. 2016) and is justified for walls undergoing significant rocking (Doherty et al.
228 2002; Griffith et al. 2003). Its application to the herein developed tri-linear model is validated in
229 this paper.

230 ### *Equation of motion*

231 Based on the above assumptions, D'Alembert's principle can be written for the wall configura-
232 tions depicted in Fig. 2. The use of this principle leads to the equation of motion for the equivalent

single-degree-of-freedom system, which writes:

$$\ddot{\Delta}(t) + \frac{C}{M}\dot{\Delta}(t) + \frac{3}{2}\frac{F(\Delta(t))}{M} = -\frac{3}{2}a_g(t). \tag{14}$$

In the above equation, $\Delta(t), \dot{\Delta}(t)$ and $\ddot{\Delta}(t)$ are respectively the displacement, the velocity and the acceleration measured at the control point of the wall, M is the total wall mass and C is the equivalent viscous damping factor. The derivation of Eq. (14), which for sake of conciseness is not reported in the paper, follows Griffith et al. (2003), where the equation was originally derived for walls where the middle crack is located at mid-height. The same equation is obtained here for an arbitrary crack location and using as control point the wall mid-height.

The response $F(\Delta(t))$ given in the equation is the time-integrated force-displacement relationship of the wall, when this latter is subjected to uniform inertia forces. In Griffith et al. (2003), the expression for $F(\Delta)$ was given by a non-linear elastic force-displacement curve of a bi-linear model. In the present case, $F(\Delta)$ is given by the developed tri-linear model. The use of a non-linear elastic force-displacement curve represent a simple yet reliable modeling assumption which, as shown in this and previous works (Doherty et al. 2002; Sorrentino et al. 2016), allows mimicking the rocking behavior of vertically-spanning, or one-way bending, URM walls. Contrarily from what observed on two-way bending walls, the experimental behavior of one-way bending walls undergoing rocking is characterized by the absence of hysteresis cycles due to damage. The response of these walls is in fact mainly governed by geometric non-linearities, the main source of damping being the impact between the macroblocks (Lam et al. 1995; Doherty 2000; Griffith et al. 2004; Meisl et al. 2007; Dazio 2009; Derakhshan et al. 2014; Ferreira et al. 2015; Graziotti et al. 2016; Giaretton et al. 2016b; Degli Abbati and Lagomarsino 2017).

Damping factor

A viscous damping factor based on a constant damping coefficient c is used for the integration of the tri-linear model. Related to the initial stiffness of the model, this factor reads (Griffith et al. 2003): $C = \sqrt{6MK_1}c$. For the simulations conducted in this paper, a constant damping coefficient

of 5% is used. This value constitutes a lower bound of the values observed during free-rocking tests (Griffith et al. 2004; Doherty 2000; Graziotti et al. 2016; Giaretton et al. 2016b). It has been shown that taking this value is a suitable choice when combining the tri-linear single-degree-of-freedom system with a viscous damping model (Griffith et al. 2003; Melis 2002), resulting in only negligible differences with respect to other more sophisticated numerical procedures such as the 'event-based' one proposed by Doherty (2000).

Model implementation

The tri-linear model is integrated numerically by means of the classical Newmark time-integration scheme. Simulations are run until failure of the wall occurs. The following failure condition is adopted:

$$|\Delta| \geq \Delta_{\mathrm{U}}. \tag{15}$$

MODEL VALIDATION

Two series of laboratory shake table tests carried out on walls undergoing rocking under out-of-plane excitations are used for validating the tri-linear model. Both test series involve single-leaf brick masonry walls spanning vertically between two supports, with top support conditions reproducing connections between the walls and reinforced concrete slabs in existing buildings (Fig. 2(a)). Section S4 of Supplemental Data gives the link to a repository containing the Matlab code used in this section for the validation of the tri-linear model.

Simulation of Adelaide tests

The walls tested at the University of Adelaide (Griffith et al. 2004; Doherty 2000) had a height $H_{\mathrm{w}} = 1500$ mm, a length $L_{\mathrm{w}} = 950$ mm and a nominal thickness of $t_{\mathrm{w}} = 110$ and 50 mm. They were made of bricks with mass densities of 1800 and 2300 kg/m^3, respectively. At their base, the walls were placed onto a straight steel plate after application of a mortar layer. At the top, the last row of bricks was laterally supported by two stiff rubber spacers fixed on both sides into L-shaped steel profiles. This prevented the lateral displacement but not the rotation of the bricks (Doherty

2000), resulting in a boundary condition similar to that at wall base, where the bricks were able to rotate after cracking of the mortar layer (Doherty 2000). In order to seize this condition, the walls are modeled as clamped at their ends: the moment originating at the wall ends leads to the partial cracking of the cross section and, as a result, the reaction force moves, as in the tested configuration, towards the compressed region of the cross-section (Godio and Beyer 2017).

Griffith et al. (2004) tested three walls under out-of-plane loading on the shake table. The two 110 mm-thick specimens 12 and 13 without overburden are selected for validating the model. The 50 mm-thick specimen 14 was also tested on the shake table but the results for this specimen are not reported (Griffith et al. 2004; Doherty 2000). For the tests, Griffith et al. (2004) used the Nahanni, El Centro and Pacoima ground motions scaled at different intensities. When simulating the tests, the actual table accelerations are used as input for the tri-linear model, except for the Pacoima ground motion scaled at 66%, for which the input motion for the tri-linear model is here derived by scaling the table acceleration of the Pacoima motion available at 80%. This approach is taken as an unrealistic low response of the tri-linear model is observed when using the recorded table acceleration for that motion, possibly due to a wrong measurement of the table acceleration.

Quasi-static pushover tests were carried out on the specimens before and after the shake table tests, to study respectively the uncracked and cracked behavior of the walls. The analytical model presented by Godio and Beyer (2017) was used to simulate the pushover tests carried out on the cracked walls and showed that an important reduction of the elastic moduli occurred due to the degradation of the joints. The resulting values of E_{m} were derived from the initial stiffness of the static force-displacement curve of the walls and were 43 and 5 MPa, respectively for specimen 12 and 13 (Godio and Beyer 2017). These values are used here for the simulation of the shake table tests by the tri-linear model. Table 2 gives the list of the force and displacement parameters used in the tri-linear model for simulating the Adelaide tests. No mortar drop-out was observed during the tests for the specimens that are here modeled. Moreover, the walls were cracked at mid-height from the previous pushover tests, where a concentrated force was applied at mid-height. In the simulations, the middle crack position is consequently fixed at mid-height and the displacement

parameter Δ_U, representative of the effective wall thickness, is set equal to the nominal wall thickness: $\Delta_U = \Delta_0 = t_w$ (Eq. (2)).

Force-displacement curves

Fig. 4 shows the comparison of the tri-linear model with the experimental results in terms of normalized dynamic force-displacement curves. The experimental curves are built following Doherty (2000), see also Graziotti et al. (2016): Δ is the relative displacement measured at the wall mid-height, where the middle crack is located, and F is the force derived by multiplying the absolute acceleration of the center of mass of the two portions of wall that are delimited by the middle crack, by their mass. To this purpose, a triangular distribution of the relative acceleration along the wall height is assumed as in Fig. 2. To be consistent with the experimental results, the numerical curves show the total inertia force, which, according to Eq. (14), is the sum of the restoring force, $3/2F(\Delta)$, and the force generated by damping, $C\dot{\Delta}$. The figure shows the accuracy of the tri-linear model and the selected damping model in reproducing the force and displacement capacity of the walls tested on the shake table. Moreover, the initial stiffness of the walls, which was back calculated starting from pushover tests (Godio and Beyer 2017), yields a good estimation of the stiffness observed in the dynamic force-displacement curves. The comparison is complemented with the results obtained from the tri-linear model built based on the empirical values proposed by Doherty et al. (2002), which were chosen on the basis of the different states of degradation observed on the same walls used for the benchmark (Griffith et al. 2003): the Δ_1/Δ_0 and Δ_2/Δ_0 ratios increased as the mortar quality degraded from new to moderately degraded and severely degraded joints, resulting in respectively $0.06; 0.13; 0.20$ and $0.28; 0.40; 0.50$. Following Melis (2002) and Griffith et al. (2003), new and moderately degraded joints are assumed respectively for specimen 12 and specimen 13, resulting respectively in $\Delta_1/\Delta_0 = 0.06$, $\Delta_2/\Delta_0 = 0.28$ and $\Delta_1/\Delta_0 = 0.13$, $\Delta_2/\Delta_0 = 0.40$. The curves given by the empirical model (Doherty et al. 2002) are very close to those given by the herein proposed tri-linear model, showing therefore good performance of this latter.

334 *Displacement time histories*

335 Fig. 5 compares the present tri-linear model and the tri-linear model proposed by Doherty
336 et al. (2002) with the experimental results in terms of normalized displacement time histories. In
337 general, the present tri-linear model shows itself able to seize the peak displacements (Table 3)
338 and the frequency content of the experimental response. Moreover, failure occurs in the test of
339 Fig. 5(b), where the specimen hits the support frame which was put in place to prevent the collapse
340 of the wall onto the shake table (Doherty 2000). For specimen 13 (Fig. 5(b),(d),(f)) the model built
341 with the empirical values proposed by Doherty et al. (2002) gives a response which is the same
342 than that of the model proposed here. For specimen 12 (Fig. 5(a),(c),(e)) the new model gives a
343 better estimate of the wall response than the empirical one, which tends to overestimates the actual
344 wall response.

345 *Error estimators*

346 The response of rocking structures such as masonry walls, columns and isolated blocks is
347 very sensitive to small changes in the geometry, the material parameters and the input excitation
348 (Psycharis et al. 2000; Papantonopoulos et al. 2002). For this reason, a full agreement between
349 numerical and experimental results can hardly be attained. Moreover, the model does not take
350 into account the wall cracking at other levels than that calculated by rigid body analysis. In
351 order to evaluate in a quantitative manner the capability of the tri-linear model in reproducing the
352 displacement time histories of the experimental response, two error estimators are used.

353 The first error estimator is denoted with $\varepsilon_{\mathrm{RMS}}$ and is based on the Root Mean Square (RMS)
354 value of the mid-height displacement computed throughout the experimental (*exp*) and numerical
355 (*trl*) time histories. It writes (Al Shawa et al. 2012):

$$\varepsilon_{\mathrm{RMS}} = \frac{|\bar{\Delta}_{exp} - \bar{\Delta}_{trl}|}{|\bar{\Delta}_{exp}|}, \tag{16}$$

with the RMS value $\bar{\Delta}$ computed over the time history $\Delta(t)$ as:

$$\bar{\Delta} = \sqrt{\frac{1}{N}\sum_{i=1}^{N} |\Delta(t_i)|^2}. \tag{17}$$

The second error estimator is based on the Weighted Mean Error (WME) and is defined as (Al Shawa et al. 2012):

$$\varepsilon_{\mathrm{WME}} = \min_{\Delta t \in [-0.50s, 0.50s]} \frac{\int_0^T |\Delta_{exp}(t) - \Delta_{trl}(t + \Delta t)\mathrm{d}t|}{\int_0^T |\Delta_{exp}(t)|\mathrm{d}t}. \tag{18}$$

This error estimator is computed by keeping fixed the experimental response and shifting the response obtained from the tri-linear model over the total duration of the time history T by a lag Δt ranging between -0.50 s and $+0.50$ s and taking the minimum WME value over this interval. This error measure can be computed taking into account either the whole time histories or, according to Al Shawa et al. (2012), only the parts of the time histories that contain displacements with amplitudes larger than 20% of the maximum absolute displacement of the experimental and numerical results (whichever is larger). All other parts of the time histories are set to zero and the error computed as defined in Eq. (18). The first method yields the error denoted with $\varepsilon_{\mathrm{WME}}$; the second yields the error $\varepsilon_{\mathrm{WME(20)}}$. The objective of these error measures is to estimate the accuracy of the tri-linear model in predicting all and large amplitude displacements not at a fixed time but within a given time window. This error proves particularly useful in the case of rocking structures, where, as already stated above, reaching a perfect agreement is practically impossible.

The errors $\varepsilon_{\mathrm{RMS}}$ and $\varepsilon_{\mathrm{WME(20)}}$ defined by Eq. (16), Eq. (18) have been used by Al Shawa et al. (2012) for estimating the sensitivity of a tri-linear model with respect to the displacement parameters Δ_1 and Δ_2, based on the comparison with experimental results. The error committed by the new tri-linear model in simulating the shake table tests presented in Fig. 5 is given in Table 3. The mean values are close to the minimum errors of $\varepsilon_{\mathrm{RMS}} = 0.300$ and $\varepsilon_{\mathrm{WME(20)}} = 0.700$, which Al Shawa et al. (2012) obtained when optimizing the displacement parameters Δ_1 and Δ_2 of his tri-linear

model. For comparison, the empirical model proposed by Doherty et al. (2002) gives errors that are on average $|\Delta_{trl}^{\max}|/|\Delta_{exp}^{\max}| = 1.207$, $\varepsilon_{\mathrm{RMS}} = 0.479$, $\varepsilon_{\mathrm{WME}} = 1.205$ and $\varepsilon_{\mathrm{WME(20)}} = 1.641$, that is approximately twice the error committed by the new tri-linear model presented here. Table 3 also contains the ratio between the absolute peak displacement measured on the tested and simulated walls: the tri-linear model yields a close and slightly over-conservative estimation of the wall peak displacements.

Simulation of Pavia tests

Graziotti et al. (2016) tested an unreinforced single-leaf brick masonry wall of $H_{\mathrm{w}} = 2754$ mm, length $L_{\mathrm{w}} = 1438$ mm and thickness $t_{\mathrm{w}} = 102$ mm. The wall was tested during an experimental campaign dedicated to the study of cavity walls. It was made of bricks with mass density $\rho = 1835$ kg/m^3 and was subjected to two levels of vertical compression stress during the tests, namely 0.3 and 0.1 N/mm^2. At its base, the wall was laid on a mortar layer placed on the foundation. At the top, the last row of bricks was fixed into L-shaped steel profiles filled with mortar, which prevented both the lateral displacement and the rotation of the bricks. Similarly to the walls tested by Doherty (2000), this wall can be modeled as double clamped, with the exception that an effective height of 2673 mm, neglecting the last row of bricks, is considered.

The specimen SIN-01-00 is used as benchmark for the tri-linear model, since it is the only one exhibiting rocking (Graziotti et al. 2016). More particularly, only the tests for which the wall undergoes mid-height displacements that are greater or equal than $0.1t_{\mathrm{w}}$ are considered. An estimate of the masonry elastic modulus can be derived from the measure of the elastic frequency of the wall, made at the beginning of the test sequence by application of a random signal. A flexural frequency of 14.27 Hz was found for the specimen SIN-01-00 (Graziotti et al. 2016). Assuming that the wall behaves at that stage as a double clamped beam made of uncracked homogeneous material, this frequency corresponds to an elastic modulus of $E_{\mathrm{m}} = 1735$ MPa, that is 0.53 times the one determined by material testing (Graziotti et al. 2016). For the simulation of tests (a)-(d) the modulus measured at the beginning of the test sequence is used. However, as the wall may lose its initial stiffness during the tests, due to the repeated shakes that damage the joints and the

units, a more precise estimate of the wall stiffness is derived for tests (e) and (f). In particular the elastic modulus is derived from the experimental $F - \Delta$ curves shown in Fig. 6. These curves were built as those of Fig. 4, i.e. taking Δ as the relative displacement measured at wall mid-height, and F as the force derived by the absolute acceleration of the center of mass of the two portions of wall delimited by the middle crack (Graziotti et al. 2016). The resulting force and displacement parameters of the tri-linear model used for simulating the Pavia tests are given in Table 4.

The comparison with the experimental curves is shown in Fig. 6 and Fig. 7. In general, the frequency content and the peak displacements (Table 5) of the experimental response are well represented by the tri-linear model (Fig. 7). The model predicts also satisfactorily the dynamic force-displacement hysteretic curves (Fig. 6). Moreover, the middle crack position predicted by the tri-linear model (Eq. (3)) is located at $0.560H_{\mathrm{w}}$ from the foundation, which is very close to the position observed in the tests of $0.575H_{\mathrm{w}}$.

The comparison with the experimental curves is complemented by the computation of the error estimators for each test (Table 5). The mean values are, also for this test series, close to the optimum values of 0.300 and 0.700 obtained by Al Shawa et al. (2012). To put the obtained error measures further in context, these error measures are also computed for the tri-linear model using the parameters suggested by Doherty et al. (2002); the new joints are assumed for tests (a) to (d) and moderately degraded joints are assumed for tests (e) and (f). The errors obtained are $|\Delta_{trl}^{\max}|/|\Delta_{exp}^{\max}| = 4.110$, $\varepsilon_{\mathrm{RMS}} = 4.186$ and $\varepsilon_{\mathrm{WME}} = 2.122$. The estimator $\varepsilon_{\mathrm{WME(20)}}$ is larger than 10 because the model predicts failure for four walls while only one wall failed during the tests.

SENSITIVITY OF MODEL PARAMETERS TO FACTORS AFFECTING THE OUT-OF-PLANE RESPONSE OF URM WALLS

An insight on the four factors affecting the response of out-of-plane vertically-spanning URM walls is carried out in this section through a sensitivity study on the tri-linear model parameters. As described in the introduction to the paper, these factors are: (a) the support conditions of the wall, (b) the level of applied axial load, (c) the height-to-thickness or slenderness ratio of the wall and (d) the deformability of the wall. The latter factor is taken into account explicitly by the tri-linear

model by taking as input the masonry elastic modulus but not its compressive strength, as it is assumed that the walls do not crush. The possibility of modeling the rounding of the unit corners due to local crushing and a reduced effective depth of the mortar layer is given by introducing an effective wall thickness as a proxy for the nominal wall thickness (Eq. (11)).

The parameters of the tri-linear model mainly depend on the P/P_{E} ratio. This ratio can be expressed in such a way that the four above-mentioned factors can be distinguished and their effect on the wall response studied separately (Godio and Beyer 2017):

$$\left(\frac{P}{P_{\mathrm{E}}}\right) = \frac{12}{\pi^2}\frac{f_{\mathrm{cm}}}{E_{\mathrm{m}}}\Lambda^2\left(\frac{P}{P_0}\right). \tag{19}$$

In the above expression P/P_0 is the axial load ratio, factor (b), with $P_0 = f_{\mathrm{cm}}L_{\mathrm{w}}t_{\mathrm{w}}$ the maximum compressive load that the wall can sustain at incipient material failure, introduced only in order to normalize the axial load applied to the wall, and f_{cm} the masonry compressive strength, which is here just assumed since not explicitly considered by the model; $\Lambda = \kappa H_{\mathrm{w}}/t_{\mathrm{w}}$ is the wall slenderness ratio, factor (c), in which the effect of the boundary conditions, factor (a), is expressed by means of κ, and E_{m} is the masonry elastic modulus, which allows studying the effect of masonry deformability, factor (d).

Effect of boundary conditions, axial load and wall slenderness ratio

Fig. 8(a) shows the variation of the force and displacement parameters of the tri-linear model versus the slenderness ratio of the wall Λ and for increasing axial loads. The figure refers to a wall strip of unitary length, height $H_{\mathrm{w}} = 2.8$ m and mass density $\rho = 1800$ kg/m^3. A compressive strength of $f_{\mathrm{cm}} = 10$ MPa and $\tau = 1$ are also assumed and E_{m} is set to 2000 MPa, which corresponds to $E_{\mathrm{m}}/f_{\mathrm{cm}} = 200$. To vary the slenderness ratio, the wall height is kept constant while the wall thickness is varied between 0.35 and 0.07m. Note that, changing t_{w} makes changing P_0 as well. Overall, increasing the wall slenderness ratio decreases the force ratio F_1/F_0 and increases the displacement ratios Δ_1/Δ_0, Δ_2/Δ_0 with an almost linear trend. The slope of the curves remains almost linear and increases with the value of P/P_0, which means that the effect of the slenderness

ratio on the model parameters is amplified by increasing axial loads. Nonetheless, already for a low axial load ratio of $P/P_0 = 0.01$, as the one that can be found at the highest levels of a building, the plateau force ranges from 0.80 to $0.95F_0$, with $F_1/F_0 \approx 0.85$ for $\Lambda = 12$. For the same slenderness but for a larger yet still relatively low ratio of $P/P_0 = 0.05$, the plateau force reduces to approximately $0.7F_0$ and for $P/P_0 = 0.10$ to $0.6F_0$. With regard to the effect of the boundary conditions, the F_1/F_0 and Δ_2/Δ_0 curves are the same for the clamped-clamped and the pinned-clamped case, since the slenderness ratio Λ is fixed at each point of the curve (Eq. (4) and (13)); on the contrary the Δ_1/Δ_0 curves result in higher ratios in the pinned-clamped case than in the clamped-clamped one, since in Eq. (12) the initial stiffness K_1 and the F_0/Δ_0 ratio are not equivalent in the two cases.

Effect of wall deformability

Fig. 8(b) shows the variation of the force and displacement parameters of the tri-linear model when varying the elastic modulus of masonry E_m, for a given compressive strength of 10 MPa, and the axial load ratio P/P_0. In this case, the slenderness ratio is fixed to 10, which corresponds to $t_\mathrm{w} = 0.14$ and 0.196 m for the clamped-clamped and the pinned-clamped case. In general, an increase of the elastic modulus leads to greater values of F_1/F_0 whereas Δ_1/Δ_0 and Δ_2/Δ_0 reduce. From the curves it is expected that for high moduli and very low axial load ratios, $(\Delta_1, \Delta_2) \rightarrow 0$ and $F_1 \rightarrow F_0$, i.e., the tri-linear model tends to the bi-linear one.

Classes of joint degradation

Fig. 8 also compares the parameters of the tri-linear model proposed by Doherty et al. (2002), who empirically distinguished new from moderately degraded and severely degraded joints, with the parameters of the herein proposed tri-linear model. With respect to the empirical values, those developed in this paper depend on the slenderness ratio, the level of applied axial load, the deformability of the masonry and the support conditions of the wall. For a given P/P_0, it can be observed that, moving from new to degraded joints, the parameters given by the present model intercept the empirical values for increasing values of slenderness and decreasing values of elastic modulus. From the comparison, classes of joint degradation to be used in the practice can be

482 distinguished.

483 CONCLUSIONS

484 Simplified tri-linear force-displacement models are an alternative to the use of refined numerical
485 simulations in the seismic assessment of vertically-spanning URM walls. Moreover, their larger
486 but still very limited number of parameters makes them very flexible compared to bi-linear models
487 derived from rigid-body analysis, which cannot capture the initial stiffness and the actual force
488 capacity of the walls (Doherty et al. 2002; Griffith et al. 2003; Sorrentino et al. 2016). The
489 deformability of the walls is a major factor in determining this latter, together with the slenderness
490 ratio and the boundary and overburden conditions of the wall (Doherty et al. 2002; Griffith et al.
491 2003; Dazio 2009; Godio and Beyer 2017). Various tri-linear models have been previously proposed
492 in the literature, but the effect of the wall deformability in conjuction with non-linear geometric
493 effects on the displacements Δ_1 and Δ_2 and therefore also on the initial stiffness K_1 and the maximum
494 force F_1 was determined by means of calibration constants determined from experimental results.
495 These constants relate the parameters of the tri-linear model to the joint conditions observed in the
496 walls (Doherty et al. 2002) or are used as correction factors for bounding the force capacity of the
497 walls obtained through bi-linear models (Derakhshan et al. 2013b).

498 In this paper, new analytical formulations for the force and displacement parameters of the
499 tri-linear model are presented. The formulations are derived from a recently developed mechanical
500 model for the out-of-plane response of URM masonry walls, in which the analytical expression of
501 the static pushover curve was given (Godio and Beyer 2017). For engineering purposes, a tri-linear
502 model is derived from the expression of the pushover curve, being particularly suited to non-linear
503 time-history analyses.

504 The tri-linear model proposed in this paper shows itself capable of providing good predictions
505 of the displacement time histories and the force-displacement hysteretic curves of tested URM
506 walls. It has the advantage of a rational development and an analytical formulation, which allows
507 covering a wide range of wall configurations. When compared to existing tri-linear models, this
508 new model needs one additional input parameter only, i.e. the elastic modulus of the masonry E_m.

Its use in the context of the seismic assessment and preliminary design of masonry buildings can be envisaged both in the modeling of the out-of-plane response of the URM walls through non-linear time-history analyses and in the prediction of the displacement demand on these walls, by means of an equivalent single-degree-of-freedom system with a secant stiffness passing through one of the points of the tri-linear curve (Godio and Beyer 2018).

NOTATION

The following symbols are used in this paper:

a_g = ground motion ($\mathrm{m/s^2}$);

C = equivalent viscous damping factor $\left(\sqrt{\mathrm{kgN/m}}\right)$;

c = damping coefficient ($-$);

E_m = elastic modulus of masonry (MPa);

F_max = force capacity of the wall (N);

F_0 = force parameter of the bi-linear model (N);

F_1 = plateau force of the tri-linear model (N);

f_cm = compressive strength of masonry (MPa);

H_w = height of the wall (m);

I_w = moment of inertia of the uncracked section of the wall ($\mathrm{m^4}$);

K_in = initial stiffness of the wall ($\mathrm{N/m}$);

K_lin = stiffness of a linear elastic Euler-Bernoulli beam ($\mathrm{N/m}$);

K_1 = initial stiffness of the tri-linear model ($\mathrm{N/m}$);

K_2 = stiffness of the equivalent single-degree-of-freedom system ($\mathrm{N/m}$)

L_w = length of the wall (m);

M = mass of the wall (kg);

O = overburden (N);

P = effective axial load of the wall (N);

P_{E} = Euler's critical load of the wall (N);

P_0 = maximum compressive load of the wall (N);

t_{w} = thickness of the wall (m);

$t_{\mathrm{w,eff}}$ = effective thickness of the wall (m);

W = self-weight of the wall (N);

$\beta, \epsilon, \kappa, \zeta$ = factors accounting for different boundary conditions (−);

Δ = displacement of the control point of the wall (m);

$\dot{\Delta}$ = velocity of the control point of the wall (m/s);

$\ddot{\Delta}$ = acceleration of the control point of the wall ($\mathrm{m/s^2}$);

$\bar{\Delta}$ = root mean square value of the displacement history (−);

Δ_{max} = displacement capacity of the wall (m);

Δ_{U} = ultimate displacement of the tri-linear model (m);

Δ_0 = displacement parameter of the bi-linear model (m);

Δ_1 = first displacement parameter of the tri-linear model (m);

Δ_2 = second displacement parameter of the tri-linear model (m);

$\varepsilon_{\mathrm{RMS}}, \varepsilon_{\mathrm{WME}}, \varepsilon_{\mathrm{WME(20)}}$ = error estimators (−)

Λ = slenderness ratio of the wall (−);

ξ = normalized position of the middle crack from the top wall support (−);

ρ = mass density of the masonry (m);

τ = ratio between effective thickness and nominal thickness of the wall (−), and

Ψ_K = function embodying $P - \Delta$ effects in the initial stiffness of the wall (−).

ACKNOWLEDGEMENTS

The work presented in this paper was founded by the Swiss Federal Office of the Environment and the Construction Department of the Canton Basel-Stadt. Additionally, the authors would like to thank Prof. Michael Griffith (University of Adelaide), Prof. Andrea Penna and Dr. Francesco Graziotti (both University of Pavia) for furnishing the dataset used for validation of the present research.

SUPPLEMENTAL DATA

Supplemental sections S1-S4 are available online in the ASCE Library (ascelibrary.org).

REFERENCES

Al Shawa, O., Felice, G., Mauro, A., and Sorrentino, L. (2012). "Out-of-plane seismic behaviour of rocking masonry walls." *Earthquake Engineering and Structural Dynamics*, 41(5), 949–968.

Brencich, A., Corradi, C., and Gambarotta, L. (2008). "Eccentrically loaded brickwork: Theoretical and experimental results." *Engineering Structures*, 30(12), 3629–3643.

Cavaleri, L., Fossetti, M., and Papia, M. (2009). "Modeling of Out-of-Plane Behavior of Masonry Walls." *Journal of Structural Engineering*, 135(12), 1522–1532.

Chapman, J. C. and Slatford, J. (1957). "The elastic buckling of brittle columns." *Proceedings of the Institution of Civil Engineers*, 6(1), 107–125.

D'Ayala, D. and Speranza, E. (2003). "Definition of Collapse Mechanisms and Seismic Vulnerability of Historic Masonry Buildings." *Earthquake Spectra*, 19(3), 479–509.

Dazio, A. (2009). "The effect of the boundary conditions on the out-of-plane behaviour of unreinforced masonry walls." *Proceedings of the 14th World Conference on Earthquake Engineering*, Beijing.

538 Degli Abbati, S. and Lagomarsino, S. (2017). "Out-of-plane static and dynamic response of masonry
539 panels." *Engineering Structures*, 150, 803–820.
540 Derakhshan, H., Dizhur, D., Griffith, M. C., and Ingham, J. M. (2014). "In Situ Out-of-Plane Testing
541 of As-Built and Retrofitted Unreinforced Masonry Walls." *Journal of Structural Engineering*,
542 140(6), 1–12.
543 Derakhshan, H., Griffith, M. C., and Ingham, J. M. (2013a). "Airbag testing of multi-leaf unrein-
544 forced masonry walls subjected to one-way bending." *Engineering Structures*, 57, 512–522.
545 Derakhshan, H., Griffith, M. C., and Ingham, J. M. (2013b). "Out-of-Plane Behavior of One-Way
546 Spanning Unreinforced Masonry Walls." *Journal of Engineering Mechanics*, 139(4), 409–417.
547 Derakhshan, H., Griffith, M. C., and Ingham, J. M. (2015). "Out-of-plane seismic response of
548 vertically spanning URM walls connected to flexible diaphragms." *Earthquake Engineering &*
549 *Structural Dynamics*.
550 Derakhshan, H., Nakamura, Y., Ingham, J. M., and Griffith, M. C. (2017). "Simulation of Shake
551 Table Tests on Out-of-Plane Masonry Buildings. Part (I): Displacement-based Approach Using
552 Simple Failure Mechanisms." *International Journal of Architectural Heritage*, 11(1), 72–78.
553 Doherty, K. (2000). "An investigation of the weak links in the seismic load path of unreinforced
554 masonry building." Ph.D. thesis, University of Adelaide, University of Adelaide.
555 Doherty, K., Griffith, M. C., Lam, N. T. K., and Wilson, J. (2002). "Displacement-based seismic
556 analysis for out-of-plane bending of unreinforced masonry walls." *Earthquake Engineering and*
557 *Structural Dynamics*, 31, 833–850.
558 Ferreira, T. M., Costa, A. A., Arede, A., Gomes, A., and Costa, A. (2015). "Experimental charac-
559 terization of the out-of-plane performance of regular stone masonry walls, including test setups
560 and axial load influence." *Bulletin of Earthquake Engineering*, 13, 2667–2692.
561 Giaretton, M., Dizhur, D., da Porto, F., and Ingham, J. M. (2016a). "Construction Details and Ob-
562 served Earthquake Performance of Unreinforced Clay Brick Masonry Cavity-walls." *Structures*,
563 6, 159–169.
564 Giaretton, M., Dizhur, D., and Ingham, J. M. (2016b). "Dynamic testing of as-built clay brick

unreinforced masonry parapets." *Engineering Structures*, 127, 676–685.

Godio, M. and Beyer, K. (2017). "Analytical model for the out-of-plane response of vertically spanning unreinforced masonry walls." *Earthquake Engineering & Structural Dynamics*, 46(15), 2757–2776.

Godio, M. and Beyer, K. (2018). "Evaluation of force-based and displacement-based out-of-plane seismic assessment methods for unreinforced masonry walls through refined model simulations." *Earthquake Engineering & Structural Dynamics*, accepted, 1–24.

Graziotti, F., Tomassetti, U., Penna, A., and Magenes, G. (2016). "Out-of-plane shaking table tests on URM cavity walls." *Engineering Structures*, 125, 1939–1947.

Griffith, M. C., Lam, N. T. K., Wilson, J. L., and Doherty, K. (2004). "Experimental Investigation of Unreinforced Brick Masonry Walls in Flexure." *Journal of Structural Engineering*, 130(3), 423–432.

Griffith, M. C., Magenes, G., Melis, G., and Picchi, L. (2003). "Evaluation of out-of-plane stability of unreinforced masonry walls subjected to seismic excitation." *Journal of Earthquake Engineering*, 7(1), 141–169.

Lagomarsino, S. (2015). "Seismic assessment of rocking masonry structures." *Bulletin of Earthquake Engineering*, 13(1), 97–128.

Lam, N. T. K., Wilson, J. L., and Hutchinson, G. L. (1995). "The seismic resistance of unreinforced masonry cantilever walls in low seismicity areas.

Landi, L., Gabellieri, R., and Diotallevi, P. P. (2015). "A model for the out-of-plane dynamic analysis of unreinforced masonry walls in buildings with flexible diaphragms." *Soil Dynamics and Earthquake Engineering*, 79, 211–222.

Lu, M., Schultz, A. E., and Stolarski, H. K. (2004). "Analysis of the Influence of Tensile Strength on the Stability of Eccentrically Compressed Slender Unreinforced Masonry Walls Under Lateral Loads." *Journal of Structural Engineering*, 130(6), 921–933.

Meisl, C. S., Elwood, K. J., and Ventura, C. E. (2007). "Shake table tests on the out-of-plane response of unreinforced masonry walls." *Canadian Journal of Civil Engineering*, 34, 1381–

1392.

Melis, G. (2002). "Displacement-based seismic analysis for out of plane bending of unreinforced masonry walls." Msc, ROSE SCHOOL, Pavia, ROSE SCHOOL, Pavia.

Morandi, P., Magenes, G., and Griffith, M. C. (2008). "Second order effects in out-of-plane strength of unreinforced masonry walls subjected to bending and compression." *Australian Journal of Structural Engineering*, 8(2), 133–144.

NTC 2008. "Decreto Ministeriale 14/1/2008. Nuove norme tecniche per le costruzioni. Ministry of Infrastructures and Transportations. Gazzetta Ufficiale della Repubblica Italiana n. 29, Supplemento Ordinario n. 30 (in Italian).

NZSEE 2014. "Assessment and improvement of the structural performance of buildings in earthquakes. Recommendations of a NZSEE Study Group on Earthquake Risk Buildings. New Zealand Society for Earthquake Engineering.

Papantonopoulos, C., Psycharis, I. N., Papastamatiou, D. Y., Lemos, J. V., and Mouzakis, H. P. (2002). "Numerical prediction of the earthquake response of classical columns using the distinct element method." *Earthquake Engineering and Structural Dynamics*, 31(9), 1699–1717.

Priestley, M. (1985). "Seismic behaviour of unreinforced masonry walls." *Bulletin of the New Zealand National Society for Earthquake Engineering*, 18(2), 191 – 205.

Psycharis, I. N., Papastamatiou, D. Y., and Alexandris, A. P. (2000). "Parametric investigation of the stability of classic al columns under harmonic and earthquake excitations." *Earthquake Engineering and Structural Dynamics*, 29(8), 1093–1109.

Sorrentino, L. (2003). "Dinamica di muri sollecitati fuori del piano come sistemi di corpi rigidi.

Sorrentino, L., D'Ayala, D., de Felice, G., Griffith, M. C., Lagomarsino, S., and Magenes, G. (2016). "Review of Out-of-Plane Seismic Assessment Techniques Applied To Existing Masonry Buildings." *International Journal of Architectural Heritage*, 11(1), 1–20.

Sorrentino, L., Masiani, R., and Griffith, M. C. (2008). "The vertical spanning strip wall as a coupled rocking rigid body assembly." *Structural Engineering and Mechanics*, 29(4), 433–453.

Tomassetti, U., Graziotti, F., Penna, A., and Magenes, G. (2018). "Modelling one-way out-of-plane

response of single-leaf and cavity walls." *Engineering Structures*, 167(February), 241–255.

Tondelli, M., Beyer, K., and DeJong, M. (2016). "Influence of boundary conditions on the out-of-plane response of brick masonry walls in buildings with RC slabs." *Earthquake Engineering & Structural Dynamics*, 45(8), 1337–1356.

List of Figures

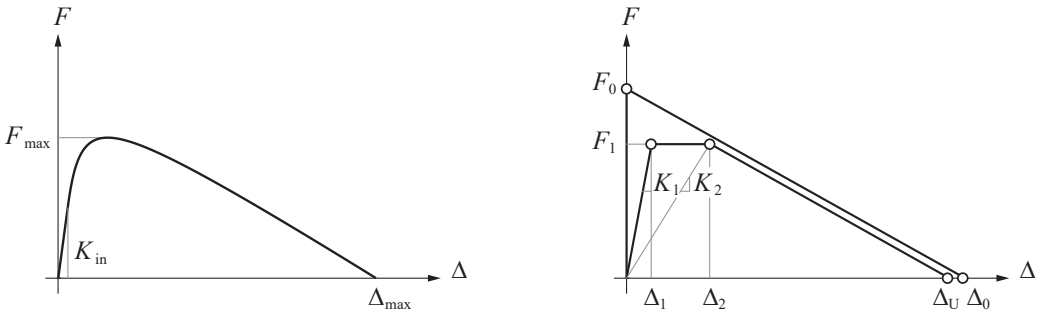

(a) Experimental curve (b) Bi- and tri-linear models

Fig. 1. Force-displacement curves and simplified models of vertically-spanning out-of-plane loaded URM walls.

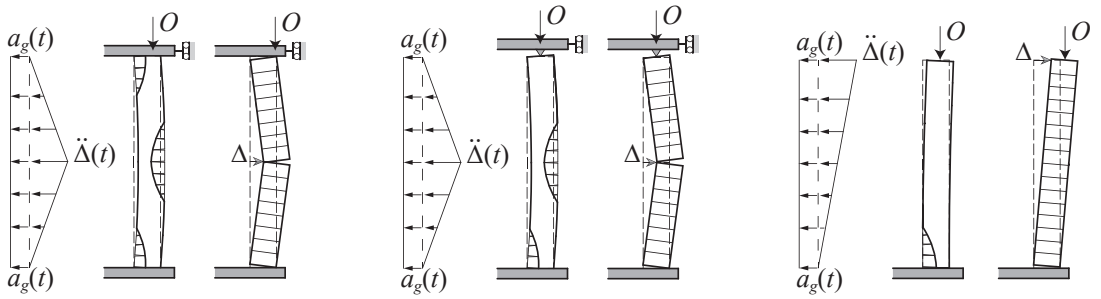

(a) Clamped-clamped (b) Pinned-clamped (c) Cantilever or parapet

Fig. 2. URM walls spanning vertically between two supports (a)-(b) or laid on one single support (c). Walls are subjected to overburden and out-of-plane loading. Piece-wise linear inertia force distribution is assumed. Deformable and rigid-body idealizations of the walls: regions in which cracking occurs are shown in the deformable case.

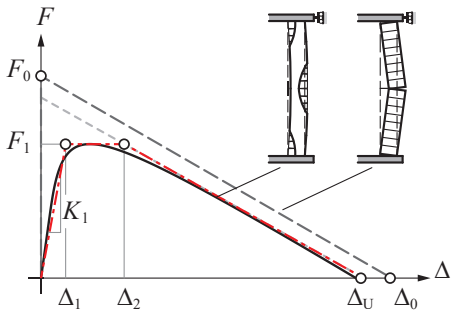

Fig. 3. Derivation of the tri-linear model (dotted-dashed line) from the bi-linear model (dashed line) and the pushover curve (solid line).

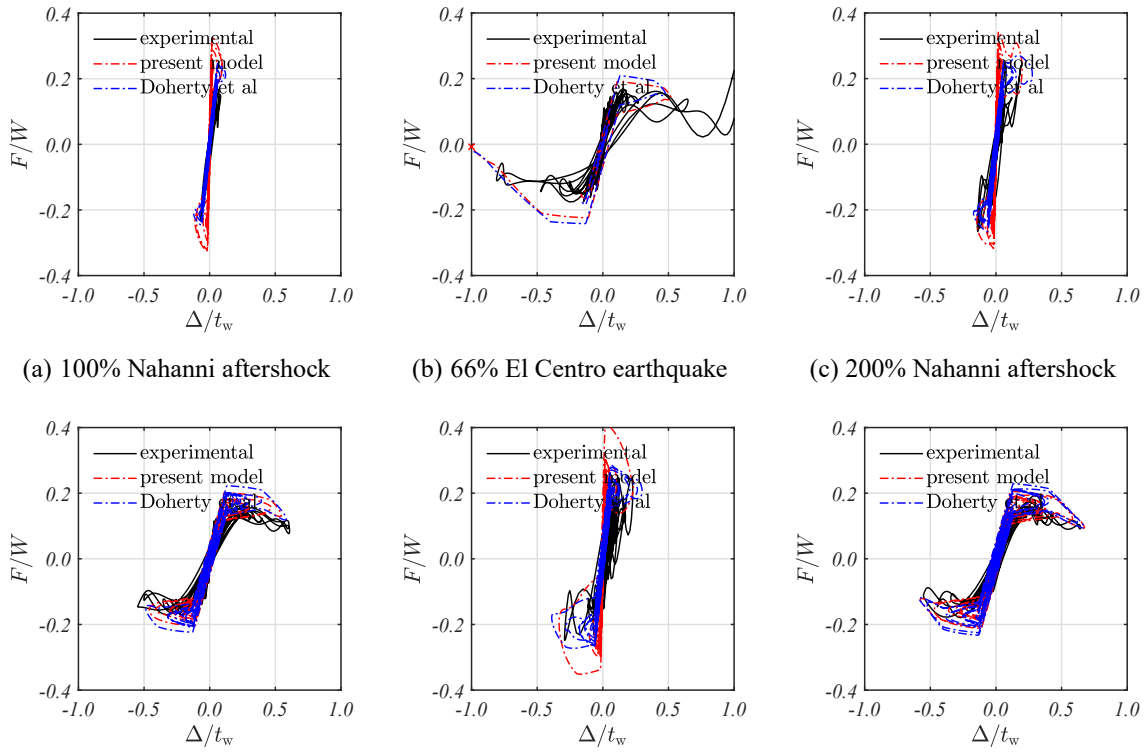

(a) 100% Nahanni aftershock (b) 66% El Centro earthquake (c) 200% Nahanni aftershock

(d) 66% Pacoima earthquake (e) 400% Nahanni aftershock (f) 80% Pacoima earthquake

Fig. 4. Simulation of the shake table tests carried out at the University of Adelaide. Dynamic force-displacement response of specimen 12 (a),(c),(e) and specimen 13 (b),(d),(f).

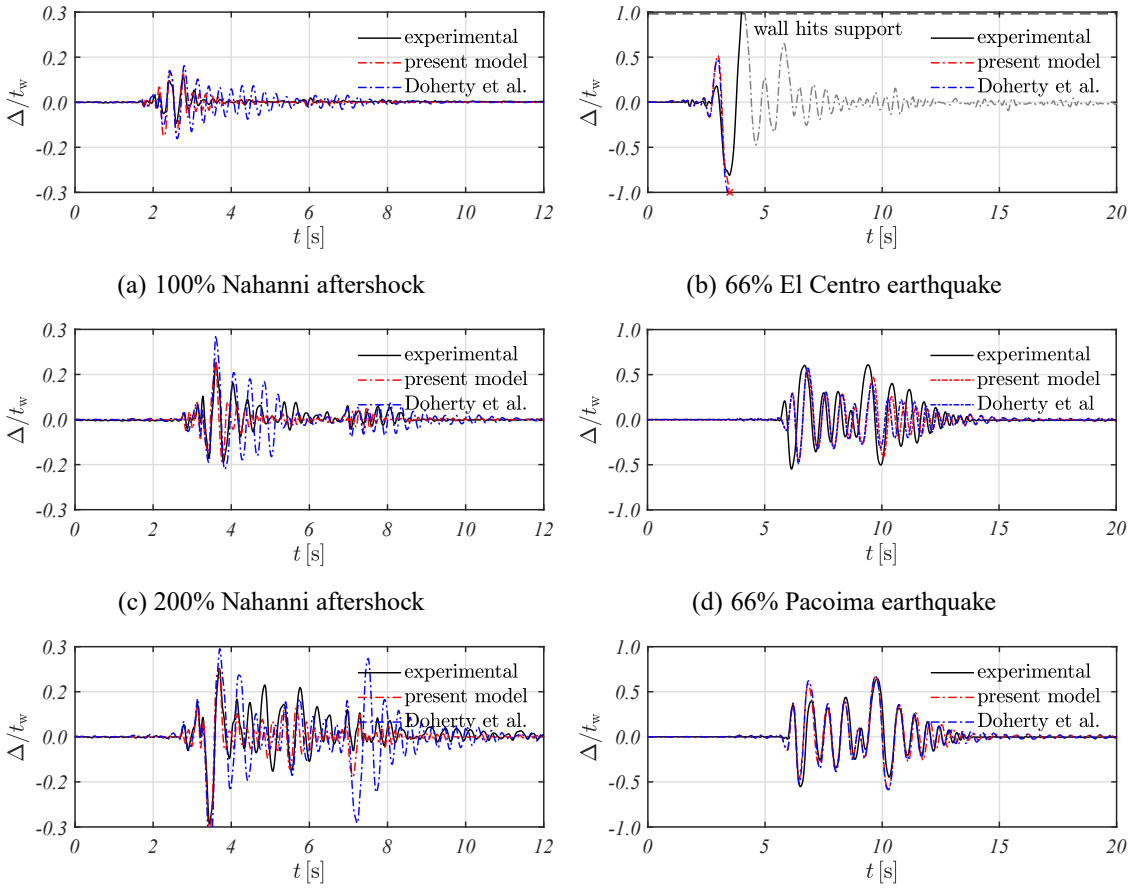

(a) 100% Nahanni aftershock

(b) 66% El Centro earthquake

(c) 200% Nahanni aftershock

(d) 66% Pacoima earthquake

(e) 400% Nahanni aftershock

(f) 80% Pacoima earthquake

Fig. 5. Simulation of the shake table tests carried out at the University of Adelaide. Displacement time histories of specimen 12 (a),(c),(e) and specimen 13 (b),(d),(f).

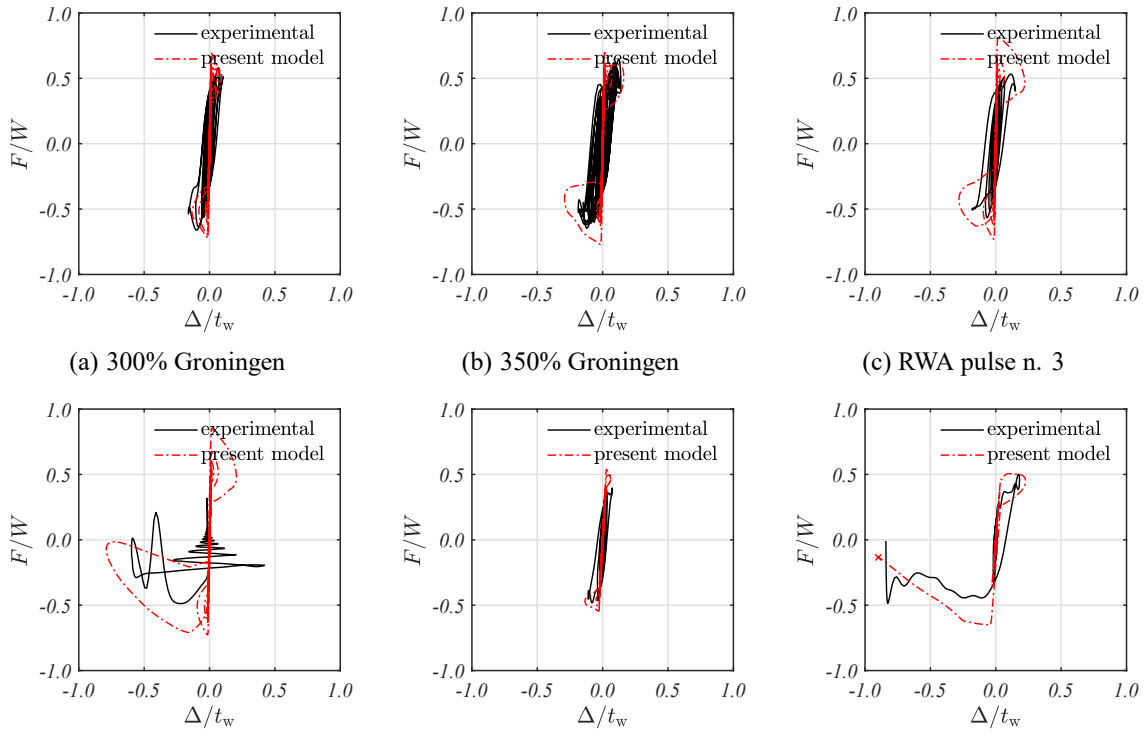

(a) 300% Groningen (b) 350% Groningen (c) RWA pulse n. 3

(d) RWA pulse n. 4* (e) 150% Groningen - artificial (f) 200% Groningen - artificial

Fig. 6. Simulation of the shake table tests carried out at the University of Pavia. Dynamic force-displacement response. *A technical issue occurred in test (d) prevented the mid-height acceleration to be measured properly (Graziotti et al. 2016).

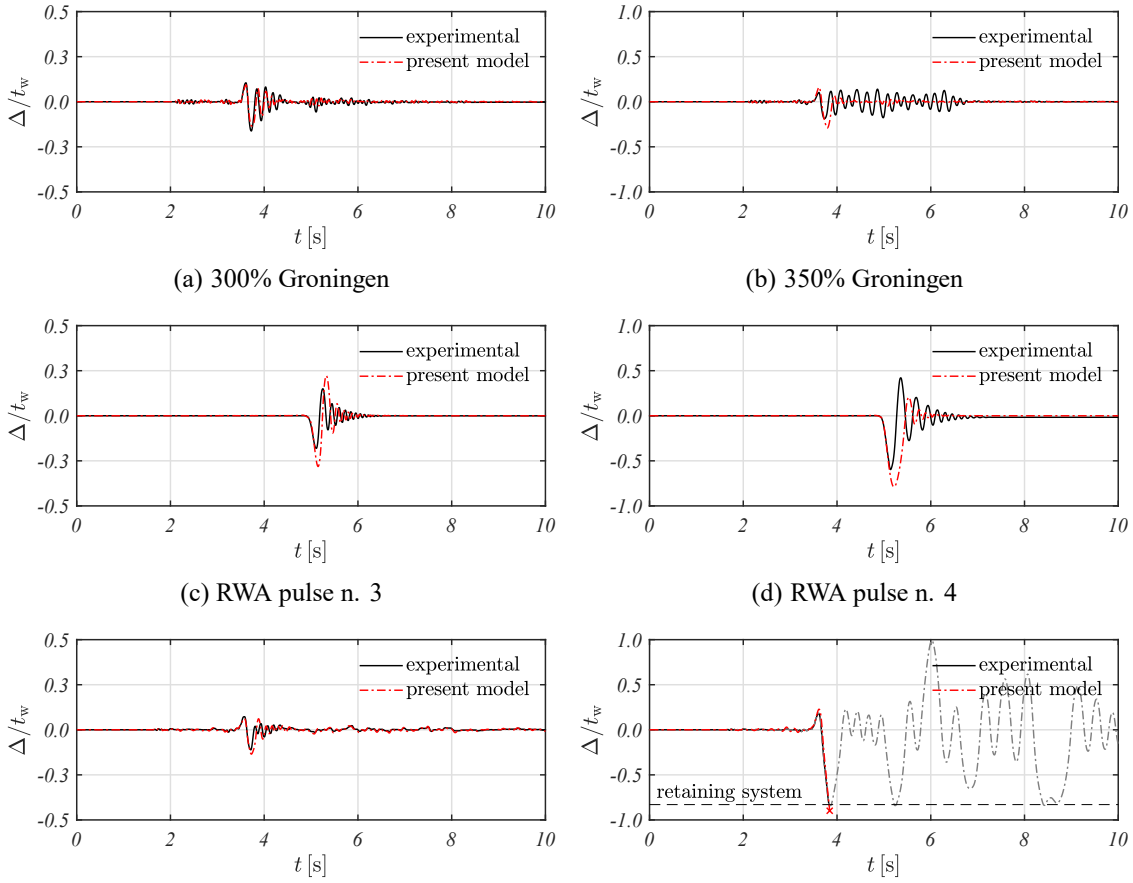

(a) 300% Groningen

(b) 350% Groningen

(c) RWA pulse n. 3

(d) RWA pulse n. 4

(e) 150% Groningen - artificial

(f) 200% Groningen - artificial

Fig. 7. Simulation of the shake table tests carried out at the University of Pavia. Displacement time histories.

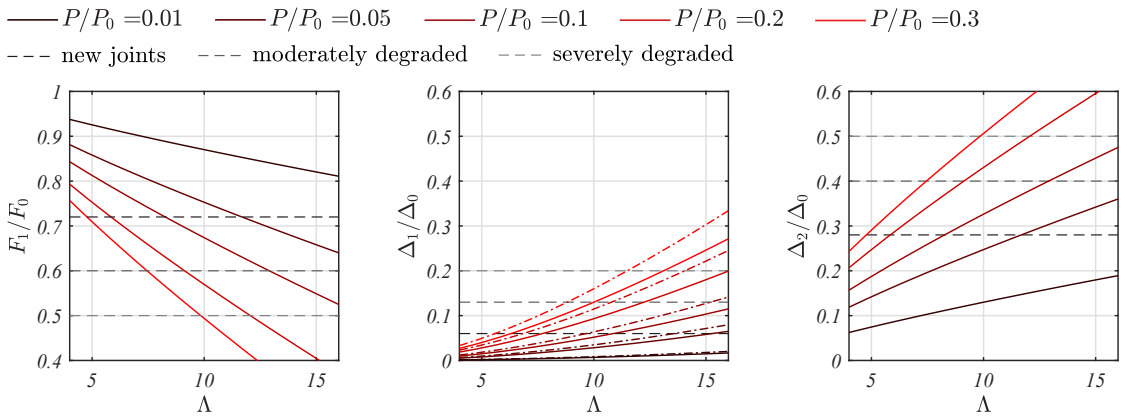

(a) Slenderness ratio $\Lambda = \kappa H_w / t_w$ (for E_m = 2000 MPa)

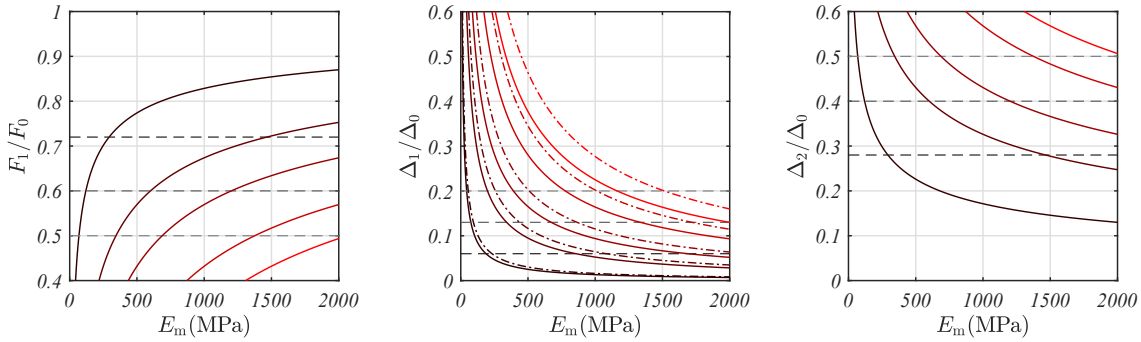

(b) Masonry elastic modulus E_m (for Λ = 10)

Fig. 8. Sensitivity study of force and displacement parameters of the tri-linear model: effect of slenderness (a) and elastic modulus (b) for clamped-clamped (solid lines) and pinned-clamped walls (dotted-dashed lines); comparison with empirical values contained in the literature (Doherty et al. 2002) for different states of joint degradation (dashed lines).

List of Tables

Table 1. Summary of existing tri-linear models describing the out-of-plane response of vertically-spanning URM walls. Support conditions of the wall (Fig. 2): CC = clamped-clamped; PC = pinned-clamped; Cant. = cantilever.

Tri-linear model	Support conditions	Joints condition	Δ_1/Δ_0	Δ_2/Δ_0	Δ_U/Δ_0	F_1/F_0
Doherty et al. (2002)	CC, PC, Cant.	New	0.06	0.28	1	0.72
		Moderately degraded	0.13	0.40	1	0.60
		Severely degraded	0.20	0.50	1	0.50
Derakhshan et al. (2013b)	PC		0.04	$1 - F_1/F_0$	≤ 1*	0.83**
Al Shawa et al. (2012)	Cant., one-side rocking		0.02	0.20-0.35	0.94	0.74-0.59
Derakhshan et al. (2015)	PC, flexible top and bottom supports		0.04	0.33	1	0.67
Landi et al. (2015)	PC***		0.05	0.26	1	0.74
Tomassetti et al. (2018)	CC, single-leaf and cavity walls		0.03-0.04	0.06-0.25	0.92-0.98	0.73-0.90

*expressed as a function of the mortar pointing and the compressive strength of the masonry

**with F_0 calculated by rigid-body analysis of the wall including the limited compressive strength of the masonry

***values given according to the formulations proposed by Sorrentino (2003)

Table 2. Parameters of the tri-linear model used for simulating the Adelaide tests. Imposed middle crack position at $0.5H_{\mathrm{w}}$.

Tested wall*	Δ_1/Δ_0	Δ_2/Δ_0	F_1/F_0
Specimen 12 (a),(c),(e)	0.017	0.198	0.802
Specimen 13 (b),(d),(f)	0.110	0.468	0.532

*reference to results contained in Fig. 4, Fig. 5

Table 3. Ratio between the absolute peak displacements and error committed by the tri-linear model in predicting the displacement time histories of the Adelaide tests.

Tested wall*	$\lvert\Delta_{trl}^{max}\rvert/\lvert\Delta_{exp}^{max}\rvert$	ε_{RMS}	ε_{WME}	$\varepsilon_{WME(20)}$
Specimen 12 (a)	1.342	0.544	1.105	1.365
Specimen 12 (c)	1.052	0.159	0.772	0.514
Specimen 12 (e)	1.141	0.180	0.855	0.632
Specimen 13 (b)	0.991	0.108	0.702	0.630
Specimen 13 (d)	0.898	0.244	0.742	0.710
Specimen 13 (f)	1.046	0.072	0.628	0.524
Mean value	1.078	0.218	0.801	0.729

*reference to results contained in Fig. 4, Fig. 5

Table 4. Parameters of the tri-linear model used for simulating the Pavia tests. Predicted middle crack position from the base support at $0.560H_w$.

Tested wall*	Δ_1/Δ_0	Δ_2/Δ_0	F_1/F_0
SIN-01-00 (a)	0.013	0.172	0.828
SIN-01-00 (b)	0.013	0.172	0.828
SIN-01-00 (c)	0.013	0.172	0.828
SIN-01-00 (d)	0.013	0.172	0.828
SIN-01-00 (e)	0.031	0.249	0.751
SIN-01-00 (f)	0.041	0.281	0.719

*reference to results contained in Fig. 6, Fig. 7

Table 5. Ratio between the absolute peak displacements and error committed by the tri-linear model in predicting the displacement time histories of the Pavia tests.

Tested wall*	$\lvert\Delta_{trl}^{max}\rvert/\lvert\Delta_{exp}^{max}\rvert$	ε_{RMS}	ε_{WME}	$\varepsilon_{WME(20)}$
SIN-01-00 (a)	0.830	0.154	0.784	0.394
SIN-01-00 (b)	1.559	0.225	1.044	1.126
SIN-01-00 (c)	1.558	0.607	0.996	1.456
SIN-01-00 (d)	1.324	0.382	0.998	1.365
SIN-01-00 (e)	1.217	0.304	1.035	0.892
SIN-01-00 (f)	1.069	0.076	0.226	0.102
Mean value	1.260	0.291	0.847	0.889

*reference to results contained in Fig. 6, Fig. 7